Revue des Composites et des Matériaux Avancés-Journal of Composite and Advanced Materials
Vol. 36, No. 1, February, 2026, pp. 133-144
Journal homepage: http://iieta.org/journals/rcma

Impact of High-Velocity on the Mechanical Properties of Aluminum Powder and Glass Fiber Composite Materials

Ihab S. Hasan[1], Muslim Ali[2*], Emad Q. Hussein[1]

[1] College of Engineering, University of Kerbala, Kerbala 56001, Iraq
[2] Prosthetics and Orthotics Engineering Department, College of Engineering, University of Kerbala, Kerbala 56001, Iraq

Corresponding Author Email: muslim.m@uokerbala.edu.iq

https://doi.org/10.18280/rcma.360113

Received: 30 November 2025
Revised: 3 February 2026
Accepted: 15 February 2026
Available online: 28 February 2026

Keywords:
high-velocity impact, aluminum powder, glass fiber composite, energy absorption, material performance, tensile strength, finite element analysis

ABSTRACT

This study investigates the high-velocity impact performance of a hybrid composite material consisting of glass fibers and aluminum powder, with epoxy as the matrix. Specimens were fabricated with varying fiber and aluminum powder content (20%-60% glass fiber, 5%-15% aluminum powder) and tested at velocities of 11.43, 16, 20, and 25 m/s using a gas gun system. The results revealed that increasing the glass fiber content significantly improved the tensile strength and impact resistance, with the best performance observed in samples containing 60% fiber. Aluminum powder addition also improved the material's impact absorption, though to a lesser extent. The experimental data were validated by finite element analysis (FEA), showing a high correlation between numerical and experimental results, with residual velocities differing by less than 10%. These findings provide valuable insights into optimizing the performance of hybrid composites for high-impact applications.

1. INTRODUCTION

The potential effectiveness of glass fibers and aluminum powder under dynamic loading, compression, and high-speed impacts, even after damage to the specimens caused by such impacts. Materials will be combined: the benefits of the glass fibers give superior tensile strength and rigidity, while toughness through energy-absorbing properties is achieved with the addition of aluminum powder. Some key studies that have furthered the knowledge base with respect to mechanical properties, processing techniques, and testing methodologies of these hybrid composites will be discussed in the following sections. The addition of aluminum powder enhanced the toughness, impact resistance, and thermal stability of such composites [1, 2]. It has performed drop-weight impact tests on aluminum-reinforced composites and found that the absorption of energy due to the addition of aluminum was significantly improved [3, 4]. It has conducted a study in which some mechanical properties (tensile, hardness, and impact strength) of ethyl silicate resin were evaluated according to standard criteria [5]. It has conducted a study that looked into the tensile properties of hybrid composites containing different fractions of aluminum powder; their work showed that with the addition of 10 % aluminum, the mechanical strength was enhanced up to 25%. Further increases in percentages revealed no significant improvement; in fact, this showed that optimization has to be done regarding aluminum content [6]. The powder metallurgy method is used to examine the roughness and hardness of the material with the addition of nanoparticles. The tensile and impact properties of hybrid composites were evaluated, and it was noted that inclusions of aluminum powder improve the load-carrying capacity of composites [7]. Composites containing 10% aluminum powder exhibited the best balance between strength and impact resistance [8]. It has investigated the effects of glass fibers aligned parallel and/or perpendicular to the thickness direction of the hybrid composite on the mechanical properties. Their observations showed that the perfect fibre alignment in the direction of applied load was improving the tensile strength and impact resistance, thus indicating that fibre direction is one of the most important parameters in designing the composites [9, 10]. It has created an impact testing set-up for assessing hybrid composites under realistic conditions. Their calibrated method gave correct information about the resistance characteristics of the impact on aluminum-reinforced composites, essential to material behavior in dynamic scenarios [11, 12]. It has conducted research on the fatigue life of hybrid composites by implementing numerical and experimental approaches through FEA. The result showed that the fatigue life improved by 20% due to the addition of aluminum powder, which enhanced the sustainability of the material when it came to cyclic loading [13, 14]. Using different-speed machinery ranges from 48 to 264 meters per minute, with the highest temperature reaching 134% [15]. Finite element analysis (FEA) was performed to simulate the strain distribution in hybrid composites subjected to impact and tensile stresses. Calculations resulted in predictions of stress concentrations at locations where failures actually did take place, further benchmarking the accuracy of FEA for improving material performance [16]. A new method has been

developed for strengthening glass fiber-reinforced composites with nanoparticles of aluminum, which has increased the impact resistance significantly. This development implies that the focus of future research should be on nanoparticle-based reinforcement for advanced composite applications [17, 18]. Hybrid fibers, made up of natural fibers, synthetic fibers, or a mixture of the two, exhibit enhanced load-bearing performance in different directions in comparison to single-fiber reinforcements [19, 20]. There has been no investigation into how various types of woven fabrics, with different configurations but the same thickness, impact absorption energy in composite materials. This research examines how the high-velocity impact from a Gas Gun affects different layers of woven fabric used as reinforcement in composite material configurations.

2. EXPERIMENTAL PROCEDURE

2.1 Materials and specimen preparation

All the specimens were composed of three main components: aluminum powder, glass fiber, and low-viscosity resin. Concentration of Al studied in three values: 5%, 10%, and 15% by volume. Each ply is represented by a layer of shell elements that are interconnected through cohesive zone elements. To accurately capture the mechanical behavior, both types of elements are assigned nonlinear constitutive laws. Continuous glass fiber and Aluminum powder with a purity of 99% were used in this study as the reinforced materials in epoxy resin. Araldite GY 257 serves as the base epoxy resin in the composite being analyzed. It is combined with a hardener, ANCAMINE 1618, in an exact ratio to guarantee ideal curing and mechanical characteristics. When mixed with epoxy, Aluminum powder is carefully integrated using defined mechanical mixing techniques. This process ensures that the powder is evenly spread throughout the matrix, attaining a uniform distribution that is essential for enhanced mechanical properties, as shown in Table 1.

Table 1. Mechanical characteristics of epoxy, fiber glass, and aluminum powder

Property	Polyepoxide	Fiber Glass	Aluminum Powder
Tensile Strength (MPa)	110	3400	47
Modulus of elasticity (MPa)	4100	72300	70000
Poisson's Ratio	0.35	0.2	0.33

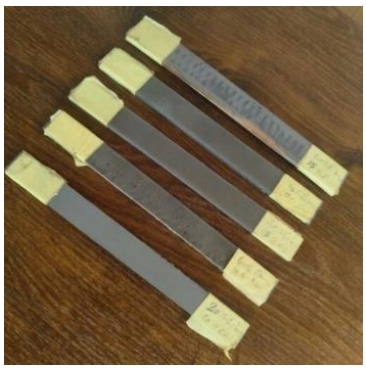

Figure 1. Tensile samples

The tensile test aimed to comprehend critical properties such as tensile strength, modulus of elasticity, and stiffness. Samples were prepared in accordance with the ASTM D3039 standard, ensuring consistency and reliability in the results, as shown in Figure 1.

The impact test was designed to evaluate the resilience and toughness of the composite materials. Conducted in accordance with the ISO-180 standard, the specimens measured 10 mm × 80 mm × 3 mm (Figure 2).

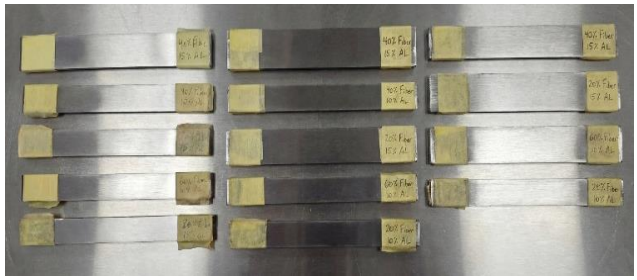

Figure 2. Impact test samples

Continuous filament fibers of glass and Aluminum powder were supplied by the University of Kerbala, College of Engineering, Mechanical Engineering Department, Iraq. Specimen preparation methods and procedures.

1. Determining the volume of each component of the specimen based on study specifications and converting it into mass calculations.
2. Put together the chamber layers and position the glass fiber layers in the chamber after ensuring they are meshed and oriented correctly as per the experimental plan (Figure 3).

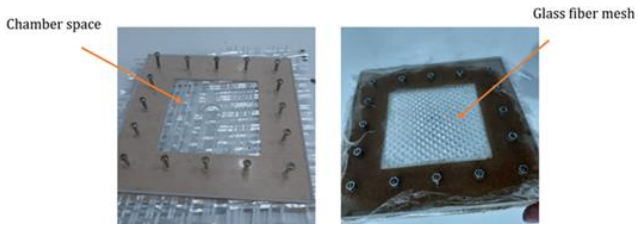

Figure 3. Assembling the chamber layers

3. Begin by combining the epoxy resin components following the guidelines provided by the manufacturer. Make sure the resin is blended in the appropriate ratio to obtain the desired characteristics, then transfer the prepared epoxy into a suitable pouring vessel.
4. Coating the fibers with the low viscosity mixed epoxy resin, ensuring they are fully saturated. Being cautious to pour the resin gently and switch containers to prevent the formation of air bubbles and spills.

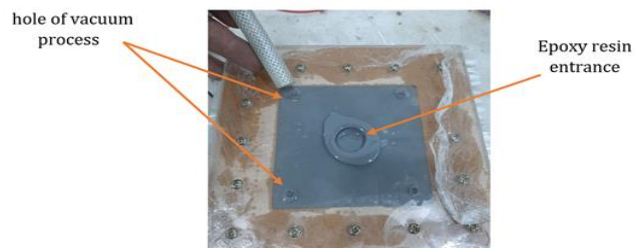

Figure 4. Pouring the resin and the vacuum process

5. Placing the chamber in a vacuum bag and using a vacuum pump to remove air, ensuring the resin fully penetrates the fibers and eliminates bubbles. Allow the composite to cure under vacuum for the recommended time at room temperature or according to the resin's specifications (Figure 4).

6. Finally, when the mixture changes to a solid state, remove the specimen shield from the chamber and trim any excess material according to specimen finishing (Figure 5).

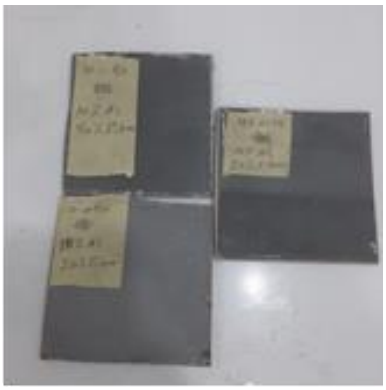

Figure 5. Specimen shields with different fiber orientations

2.1.1 Equipment Utilized in Sample Preparation

The preparation of the composite samples necessitated the use of specialized equipment, each playing a crucial role in ensuring precision, uniformity, and safety during the formulation process. The following equipment was employed:

Precision Scale

Figure 6 shows a sophisticated instrument designed for meticulously measuring mass across a spectrum from kilograms to micrograms. Due to its high sensitivity and accuracy, careful handling and calibration are imperative. Precision scales are typically an investment, reflecting their importance in ensuring exact measurements.

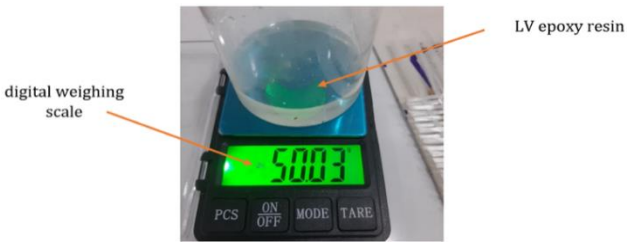

Figure 6. Precision scale

Ultrasonic Dispersion Machine

Figure 7 shows an Ultrasonic Dispersion Machine, which is vital for achieving a uniform dispersion of nano-sized particles within various solvents, such as water, oil, or resin. The machine employs ultrasound waves to effectively break down and disperse particle agglomerates, ensuring a consistent and homogenized mixture.

Evaporator

Utilized for the evaporation of acetone in the epoxy-graphene mixture, the evaporator operates by heating water to approximately 70℃ to expedite the evaporation process. This ensures that the remaining blend is devoid of any solvent residues, as shown in Figure 8.

Figure 7. Ultrasonic dispersion machine

Figure 8. Evaporator

Mechanical Mixer

Figure 9 shows an advanced piece of equipment engineered for the thorough blending of materials with varied constituents. It is particularly indispensable when dealing with nanomaterials suspended in acetone, ensuring a homogenous and consistent mixture by facilitating rigorous mixing.

Extraction Hood

The extraction hood is essential for controlling and minimizing dust emissions from nano-materials. Functioning akin to a vacuum, it guarantees a clean and dust-free working environment, thereby safeguarding both the integrity of the sample and the health and safety of the personnel involved, as shown in Figure 10.

Figure 9. Mechanical mixer

Figure 10. Extraction hood

2.1.2 Scanning Electron Microscopy

Scanning Electron Microscopy (SEM) was employed to meticulously observe the distribution of aluminum particles within the epoxy matrix. The uniformity in the distribution of aluminum particles is pivotal, as any agglomeration or clustering can significantly alter the composite's properties. SEM images provide a visual confirmation of the dispersion quality, identifying any inconsistencies or anomalies in the distribution, as shown in Figures 11 and 12.

Upon meticulous examination of the composite's fracture surfaces, the SEM images revealed the following: A generally uniform distribution of aluminum particles within the epoxy matrix was observed, adhering to our initial expectations. However, certain areas exhibited minor agglomerations, which might have potential implications for the composite's overall mechanical properties. The fracture mode appeared predominantly brittle in nature, suggesting the influence of the aluminum particles on the matrix's ductility.

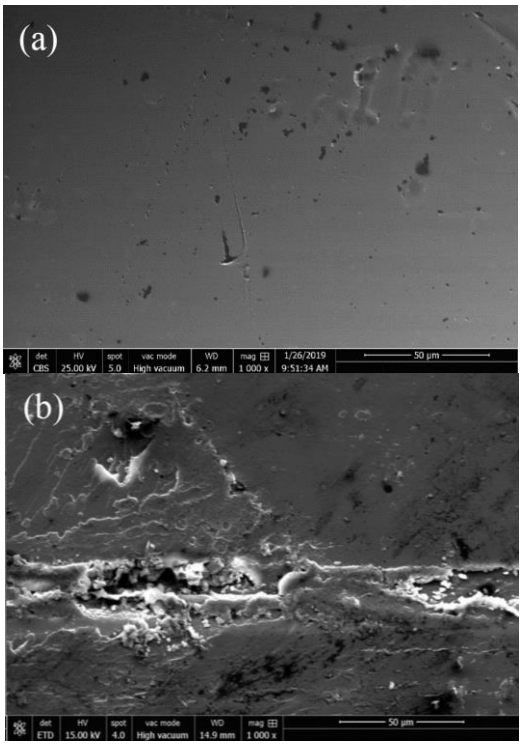

Figure 11. Scanning Electron Microscopy (SEM) photographs showcasing the fracture surfaces of the epoxy (a) 40% glass fiber and (b) 40% glass fiber and 15 % aluminum powder

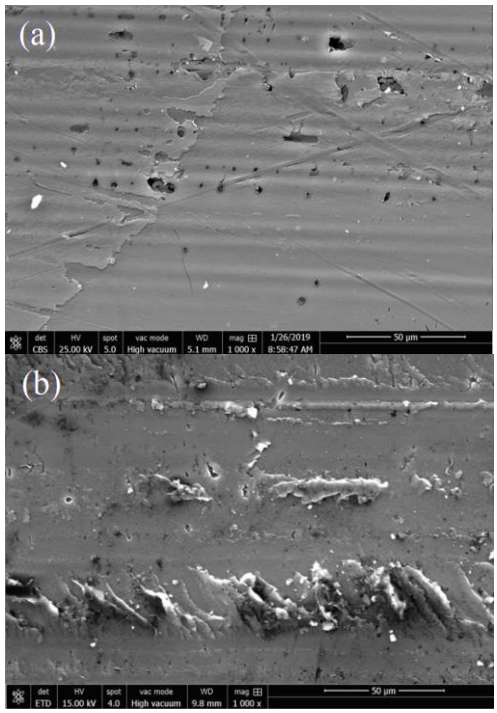

Figure 12. Scanning Electron Microscopy (SEM) photographs showcasing the fracture surfaces of the epoxy (a) 60% glass fiber and (b) 60% glass fiber and 15 % aluminum powder

2.2 Tester components

Tester device components can be classified into two types:

2.2.1 Structural and control components

Main Frame Structure

The primary structure of the apparatus consists of a robust metal frame constructed from corrosion-resistant steel to ensure rigidity and stability during testing. Designed as an elevated table, the frame possesses the following dimensions: a total height of approximately 1.2 meters, a tabletop width of 0.8 meters, and a depth of 0.6 meters. This configuration provides ample space for the secure installation of all components, as illustrated in Figure 13.

Figure 13. Main frame structure

Launch Tube

The launch tube constitutes a crucial component of the test

(Figure 14). It comprises a DN12.5 mm (0.5-inch) diameter and a length of 750 mm (30.48-inch) PVC wall with a thickness of 3 mm. PVC wall was chosen to reduce inside heat and friction losses, which effects on projectile mass velocity. Furthermore, PVC Tube ensures compatibility with electrical sensors' work and prevents any magnetic field interference with the shooting steel mass process that could affect velocity measurement accuracy. The launch tube is mounted horizontally and securely, ensuring direct alignment with the specimen's center. Sturdy supports and brackets, along with clamps and metal fasteners, ensure the tube's stability and testing safety. This robust mounting system allows for multiple tests without requiring tube repositioning, contributing to consistent and accurate results.

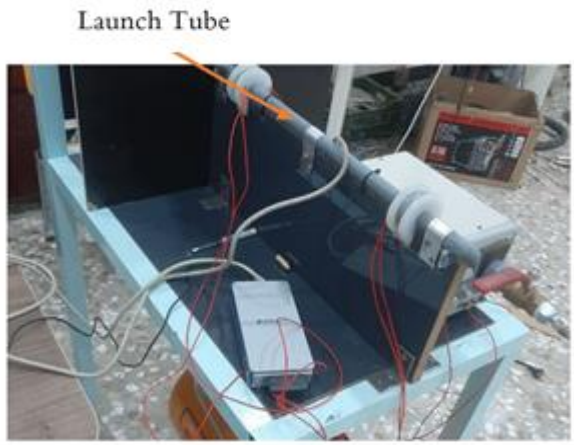

Figure 14. Launch tube

Pressure System

The INGCO 50L (AC25508) air compressor, shown in Figure 15 used in this study. It's served as a fundamental component in this experiment. It's operating at 1.8 kilowatts (2.5 horsepower) electrical motor with a rotational speed of 2850 revolutions per minute, the compressor efficiently generates high volume and air pressure for only by some minutes. One of the key advantages of this compressor have dual pressure gauges. The first gauge monitors pressure within the tank, while the second gauge measures pressure in the launch tube. This setup allows the compressor to incorporate a pressure regulator, enabling users to fine-tune the desired pressure, making it ideal for shooting a 30-gram cylindrical steel mass with controlled velocity. The compressor features a 50-liter tank, providing ample capacity to ensure a continuous and stable airflow during experiments.

Figure 15. INGCO 50L (AC25508) air compressor

Valves and Connecting Pipes

The testing apparatus features an extensive network of pipes and valves to facilitate accurate regulation of compressed air flow during evaluations, as shown in Figure 16. A strengthened, flexible plastic line links the compressor tank to the launch tube, allowing for essential mobility and enduring high pressures of up to 8 bar. The flexibility of this hose renders it appropriate for experiments with frequent modifications to component placement. There is a ball valve fitted at the terminus of this hose, which boasts high-class sealing properties. Turning the valve after it has been attached to the launch tube allows one to safely release the pressure and move the projectile onto the specimen. The pressure emanating from the hose into the launch tube is effectively directed, at the same time offering total control of the launch process. The compressor also includes a set of valves for the regulation of airflow and pressure within the enclosed system. These valves are applied to retain pressure within the system as it gets prepared for equipment launch. At the time of end testing, pressure can be released from the system through a control device located above the compressor. This control device includes a mechanism especially for the safe release of pressure effectively. This integrated system of pipes and valves provides comprehensive control over pressure flow, ensuring safe and precise experimental procedures.

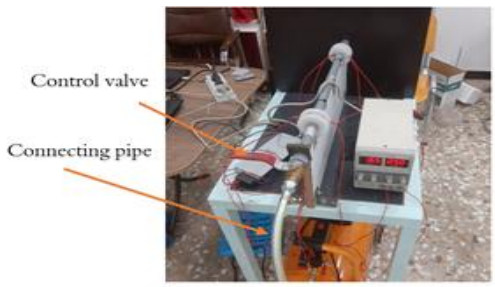

Figure 16. Valves and connecting pipes

Figure 17. Specimen clamping mechanism

Specimen Clamping Mechanism

The specimen clamping mechanism is meticulously designed to ensure high-precision impact testing of the specimen. It consists of a supporting wall fitted with two walls constructed from wood and PVC foam, simulating the effect of a hanging specimen (Figure 17). These resilient, impact-absorbing materials aim to replicate the behavior of real-world structures subjected to sudden forces, thereby providing a test environment that closely resembles actual conditions. The specimen is securely fixed opposite the launch end nozzle to repel the projectile metal cylinder. The two damping walls installed behind the specimen help support it while not affecting the impact energy. Wood supporting wall, directly connected to the frame. The foam supporting wall is glued over the first wall wood support. The specimen is hung over the foam support. This support mechanism provides the

necessary stability for the clamping process and ensures the safety test, even at high launch velocities. Also, this design guarantees a uniform force distribution across the specimen and prevents any movement or exposure to external factors or reactions that could influence the test results.

2.2.2 High velocity measurement instruments

Motion Sensors

The projectile mass velocity measurement system utilizes two electrical motion sensors mounted at either end of the launch tube. Each sensor comprises two coils: the first coil connects to the power supply unit with 12 V DC to generate the magnetic field inside the lunch tube. The second coil connects to the data acquisition chassis port for the signal to be recorded. Suitable distance (40 cm) chosen as time-calibrated distance between the first and second sensor. The principle of operation of the motion sensor, when a metal mass moves across a cross-stationary magnetic field made by the first coil, result fluctuation magnetic field over the second coil in the same sensor, generating an induced electrical pulse. LabVIEW signal express program employed to monitor the sensors' induced pulse.

LabVIEW Equipment kit

Figure 18 shows the National Instruments data acquisition kit type NI-DAQ 1919 chassis and cDAQ 9215 driver system employed to monitor sensor signals and record time. The one-slot Compact cDAQ-9191 Ethernet/wireless chassis is intended for use alongside C Series modules. This cDAQ chassis can accurately measure a wide variety of analog and digital I/O signals and sensors with microsecond precision. As the projectile mass passes through the first sensor, the induced signal and its time are recorded. Upon reaching the second sensor, the time is logged again. Using the time difference between the two sensors and the fixed distance between them, the projectile's velocity is precisely calculated.

Figure 18. LabVIEW equipment kit

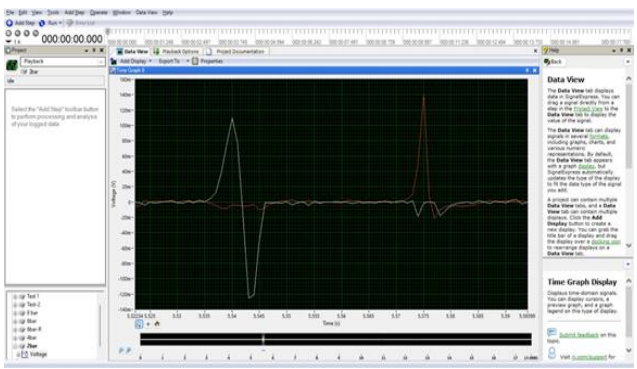

Figure 19. LabVIEW signal express program

LabVIEW Signal Express Program

In the present study, LabVIEW Signal Express program trigger functions have been used to control time and measurement of projectile mass velocity. LabVIEW Signal Express program is completely compatible with the hardware of National Instruments data acquisition chassis and drivers. LabVIEW program has an intelligent oscilloscope screen that can monitor multiple signals and record them in real time in the same test. LabVIEW program can be calibrated to measure multiple parameters such as pressure, temperature, voltage, and current, as shown in Figure 19.

3. RESULTS AND DISCUSSION

3.1 Tensile test results

Figure 20 shows the influence of Aluminum content (5%, 10%, 15%) with 20% Glass fiber. Increasing the aluminum content from 5% to 15% results in a noticeable increase in tensile strength. The specimen with 15% aluminum powder exhibited the highest peak tensile force, reaching approximately 381 MPa, followed by the 10% and 5% specimens. The deformation at break was similar for all three specimens, suggesting that while aluminum enhances strength, it does not significantly affect the specimen's ductility. For specimens with a constant 20% glass fiber content (Figure 20), the increase in tensile strength with higher aluminum content can be attributed to15%. However, the ductility remains largely unaffected in this specific series, as the glass fiber content is fixed, and the glass fiber content remains constant at 20% in these three specimens." The explanations for Figures 21 and 22 are the same. One plausible explanation could be the weak bonding between the aluminum particles and the matrix, potentially compromising the tensile strength. Alternatively, the inherent properties of aluminum powder, such as its ductility, might be affecting the composite's overall tensile behavior.

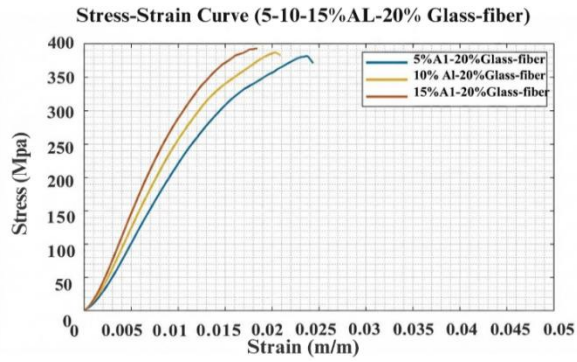

Figure 20. Experimental tensile stress – strain curves for the specimen have a constant 20% glass-fiber and (5%, 10%, 15%) Al

Figures 21 and 22 illustrate the Influence of Aluminum content (5%, 10%, 15%) with 40% and 60% Glass fiber, respectively. The tensile performance of the specimens with varying Aluminum content (5%, 10%, and 15%), while keeping the Glass fiber content constant at 40%. The results clearly show that higher Aluminum content significantly enhances the tensile strength for both 40% and 60% Glass fiber. The specimen with 15% Aluminum exhibited the highest tensile strength of nearly 650 MPa for 60% Glass fiber, while

the tensile strength of approximately 510 MPa was obtained for 40% Glass fiber, followed by the 10% and 5% specimens. The addition of glass fibers reinforces the composite, as glass fibers are well-known for their high tensile strength. This leads to a stiffer and stronger material capable of withstanding higher tensile forces. The 60% glass fiber content appears to be the optimal ratio for achieving maximum tensile strength while maintaining a balance with aluminum content.

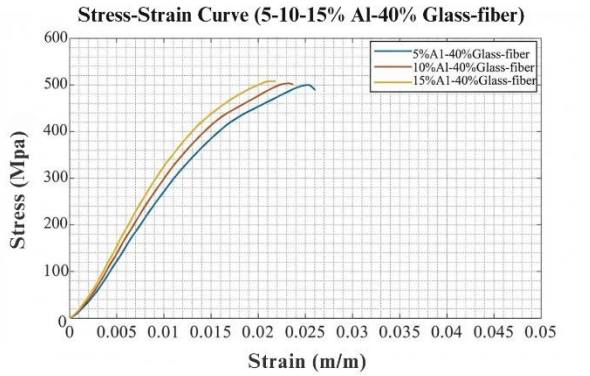

Figure 21. Experimental tensile stress – strain curves for the specimen have a constant 40% glass-fiber and (5%, 10%, 15%) Al

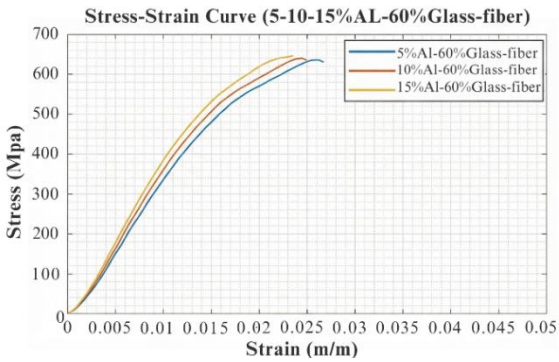

Figure 22. Experimental tensile stress – strain curves for the specimen have a constant 60% glass-fiber and (5%, 10%, 15%) Al

3.2 Modulus of elasticity

The modulus of elasticity for the composite specimens was calculated and is shown in Figure 23. The results indicate a direct correlation between glass fiber content and the modulus of elasticity, with higher glass fiber percentages resulting in higher stiffness. The inclusion of glass fibers significantly increases the modulus of elasticity, which is expected due to the inherent stiffness of glass fibers. Additionally, the presence of aluminum powder contributes to an increase in the stiffness of the composite, though to a lesser extent compared to glass fibers. The sample containing 15% Aluminum demonstrated the highest modulus of elasticity at nearly 52 GPa for 60% Glass fiber. A modulus of elasticity around 49 GPa was achieved with 40% Glass fiber, while a value of 46 GPa was recorded for 20% Glass fiber.

3.3 Impact test results

3.3.1 Projectile velocity and impact force

The calibration of the projectile velocity and corresponding impact force is presented in Figures 24 and 25. As the shooting pressure increases, the projectile velocity increases proportionally, leading to higher impact forces on the specimens. This setup was crucial for ensuring that the impact tests accurately simulated real-world dynamic loading conditions.

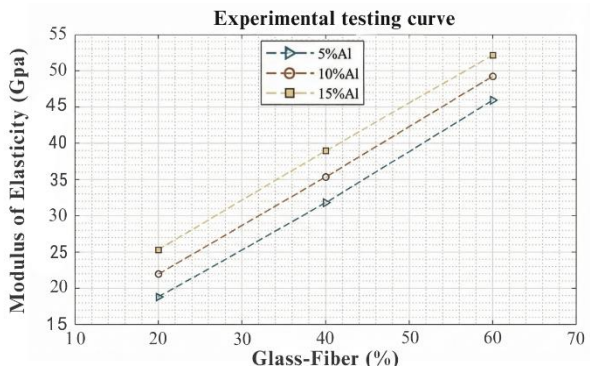

Figure 23. Experimental calculation of modulus of elasticity for composite specimens with variable percentages of glass fiber, Aluminum powder and low viscosity resin

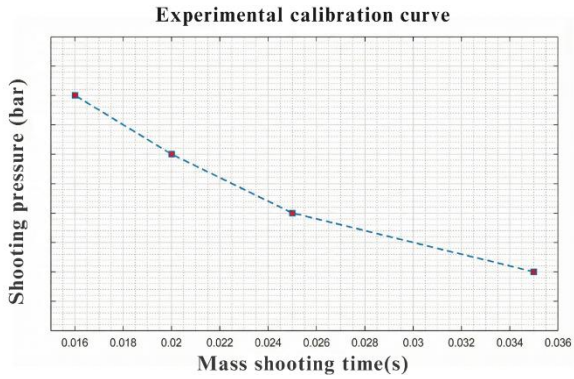

Figure 24. Experimental calibration curve to calculate the mass shooting time over two sensors distance of 0.4 m

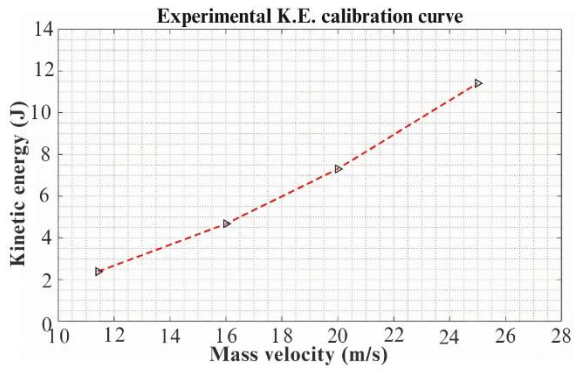

Figure 25. Experimental calibration curve to calculate the kinetic energy of the shooting mass (37.5 g) at the exit sensor

Figure 26 presents the hemispherical imprint generated on the specimen surface after impact, mirroring the projectile's head geometry.

There are three assumptions to calculate results: Assuming constant kinetic energy of the projectile mass, neglecting the effect of sample stiffness and vibration, and assuming the homogeneous deformation area can be measured. The shape of the head of the projectile mass is a hemisphere; the shape of the deformed area is a cap of a hemisphere, which can be calculated by measuring depth (h) only, as defined in Figures

27 and 28. Figure 27 demonstrates the theoretical procedure for calculating the spherical cap surface area as a function of impact depth.

Figure 26. The shape of the experimental deformation area made by the impact shock

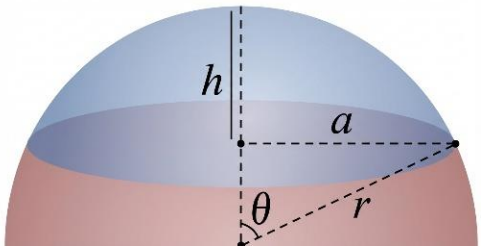

Figure 27. Theoretical calculation of the size of the spherical cap area by the depth (h)

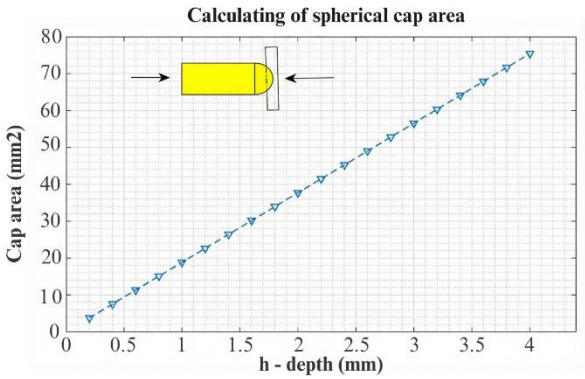

Figure 28. Range of calculation of the size of spherical cap area by depth (h)

Figure 28 provides the mathematical relationship for estimating the cap area of the spherical indentation from the measured depth.

Figure 29 shows the shape of a real tool used to measure the depth of the cap area from the surface of the sample after deformation. This device has accuracy measurements in 0.01 millimeters with a range of 0-25 mm.

Figures 30-32 show the size of the deformed cap area resulting from each sample model after being hammered by a projectile mass with four velocities (11.43, 16, 20, and 25 m/s) or equivalent kinetic energy. Results show concentration of glass fiber has a great improvement in the value of shock resistance and reduces the size of the deformed cap area. While the concentration of aluminum powder has effect lower than glass fiber concentration on the size of the deformed cap area. A significant increase in impact strength is noted when the aluminum content is raised to 15%, particularly highlighted in the findings from the 60% glass fiber, as illustrated in Figure 22. This suggests that the aluminum proportion is crucial to the overall strength of the composite.

Figure 29. Digital micrometer tool for surface depth measurement that is used to measure impact depth (h)

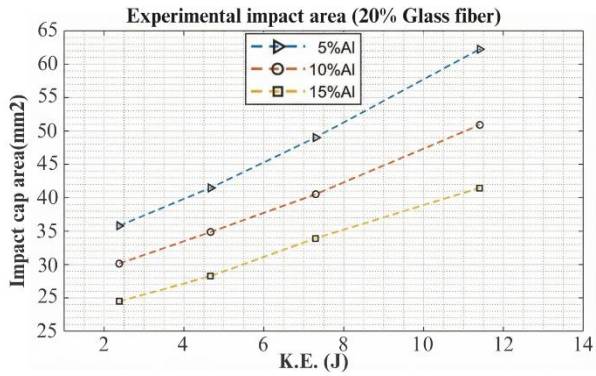

Figure 30. Experimental size of cap area which was measured on composite specimens consist of 5-10-15%Al and a constant 20% glass fiber

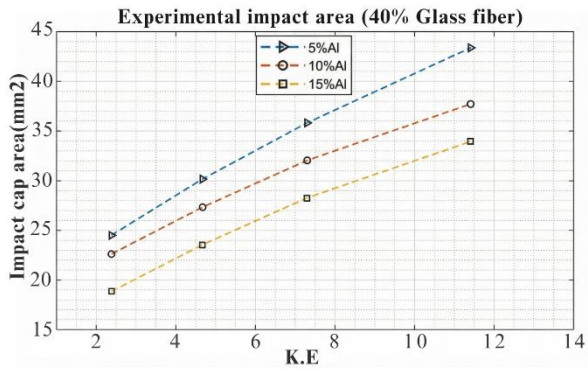

Figure 31. Experimental size of cap area which was measured on composite specimens consist of 5-10-15%Al and a constant 40% glass fiber

Figure 33 illustrates the theoretical correlation between impact stress and cap area, demonstrating an inverse trend: at constant kinetic energy, larger stresses are associated with smaller indentation areas. After recording the size of the cap area for each sample model under different conditions, impact stress can be calculated for each case by calculating the energy absorbed by the sample from this definition:

$$KN_{absorbed} = KN_{projectile} \quad (1)$$

$$Impact\ force \times depth(h) = KN_{projectile} \quad (2)$$

$$Impact\ force = \frac{KN_{projectile}}{depth(h)} \quad (3)$$

$$Impact\ stress = \frac{Impact\ force}{cap\ area} \quad (4)$$

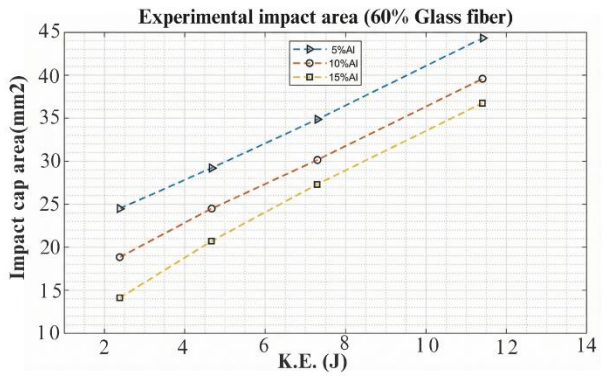

Figure 32. Experimental size of cap area which was measured on composite specimens consist of 5-10-15%Al and a constant 60% glass fiber

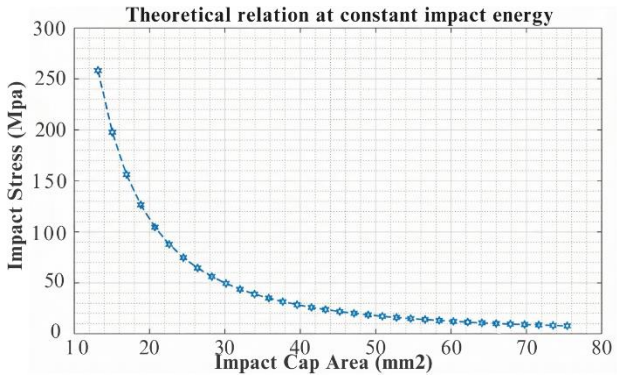

Figure 33. Theoretical relation between impact stress and impact area at constant impact energy

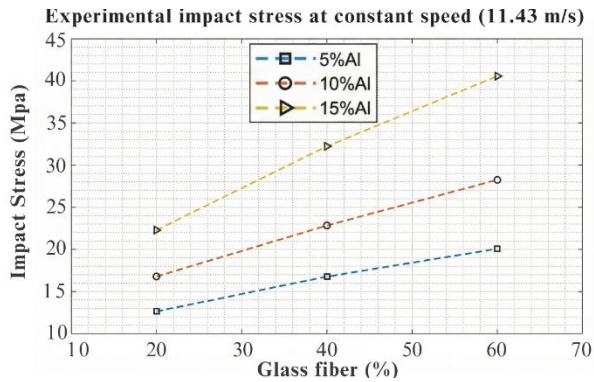

Figure 34. Experimental impact stress with variable glass fiber and Al percentages calculated at a constant projectile speed of 11.43 m/s

Results show an inverse relationship between impact stress and affected cap area at constant projectile energy. When the cap area increases, the impact stress decreases, and vice versa. That means the mean value of impact stress increases when the size of the deformed cap area decreases, referring to the sample model that is more rigid or stiff. While the value of impact stress decreases when the size of the deformed cap area increases, the sample model is more malleable or squeezable. Figures 34-37 summarize the impact stresses obtained at a constant projectile velocity across different composite configurations. The impact strength of various samples containing different percentages of powder aluminum was measured. The study focused on three specific weight percentages: 5%, 10%, and 15% of powder aluminum, tested at varying velocities. A clear pattern emerges, indicating that raising the percentage of aluminum, combined with 60% glass fiber, enhances the impact strength. The peak impact strength recorded is 108 MPa at a constant projectile velocity of 25 m/s, as illustrated in Figure 30, implying that this configuration offers the highest resistance to impact.

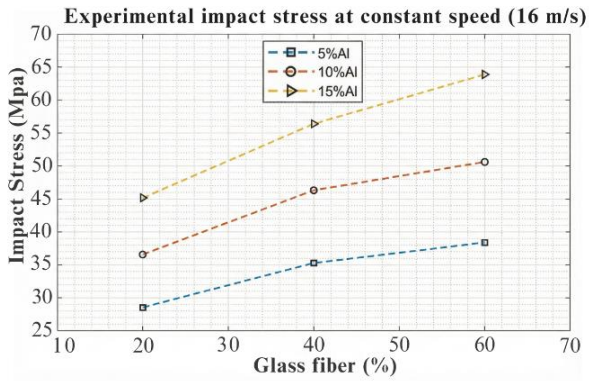

Figure 35. Experimental impact stress with variable glass fiber and aluminum percentages calculated at a constant projectile speed of 16 m/s

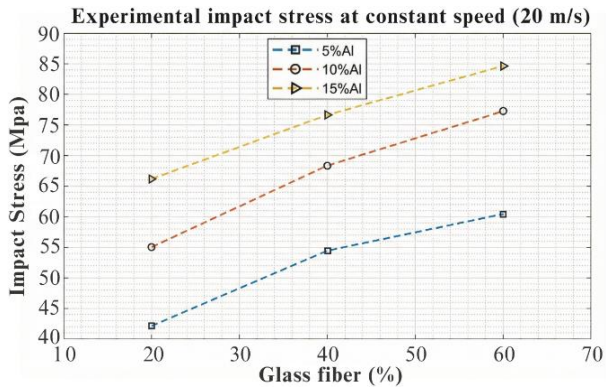

Figure 36. Experimental impact stress with variable glass fiber and aluminum percentages calculated at a constant projectile speed 20 m/s

Contrary to the tensile results, the impact strength analysis painted a favorable picture for aluminum inclusion. The impact strength consistently improved with increasing aluminum concentrations across all tested angles. Notably, the 0-90° orientation always demonstrated the highest strength, potentially due to the orientation's inherent resistance to impact. The considerable strength jumps between 10% and 15% aluminum concentrations hints at aluminum's crucial contribution to the composite's impact resistance. While aluminum enhances the impact strength, its addition also increases voids and reduces tensile strength. An optimal concentration of aluminum needs to be identified that balances

these trade-offs for desired application requirements.

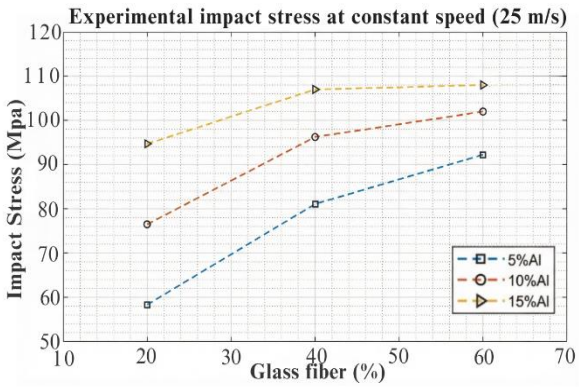

Figure 37. Experimental impact stress with variable glass fiber and aluminum percentages calculated at a constant projectile speed 25 m/s

3.4 Theoretical simulation results

Stress concentrations in certain areas, especially non-uniform distributions, might lead to potential failure points. The maximum observed stress value, if close to the material's yield strength, is concerning. Figures 38-41 show theoretical simulation results for a composite specimen impacted by a metal mass with different velocities to calculate impact stress. The simulations closely align with the experimental results, confirming that the composite specimens, which consist of 15% aluminum powder and 60% glass fiber, shot by a metal mass with various velocities, are better able to withstand high-velocity impacts. This highlights the importance of fiber reinforcement in enhancing the impact resistance of the composite material. Stress concentrations in certain areas, especially non-uniform distributions, might lead to potential failure points. The maximum observed stress value, if close to the material's yield strength, is concerning. Significant stress concentration in the middle of the object indicates potential failure zones. These areas might require reinforcement or design optimization.

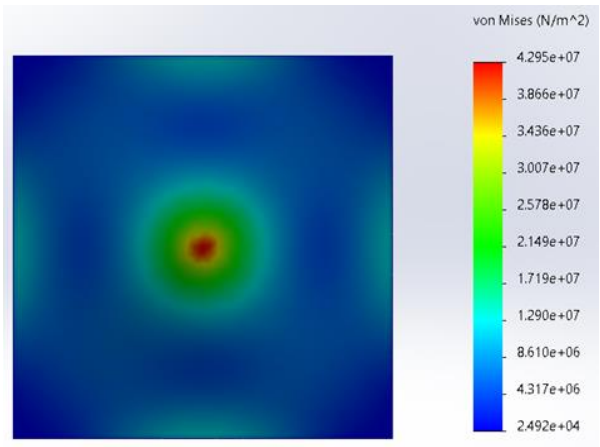

Figure 38. Theoretical simulation results for the composite specimen consist of 15% aluminum powder and 60% glass fiber, shot by a metal mass with a velocity of (11.43 m/s) to calculate the impact stress

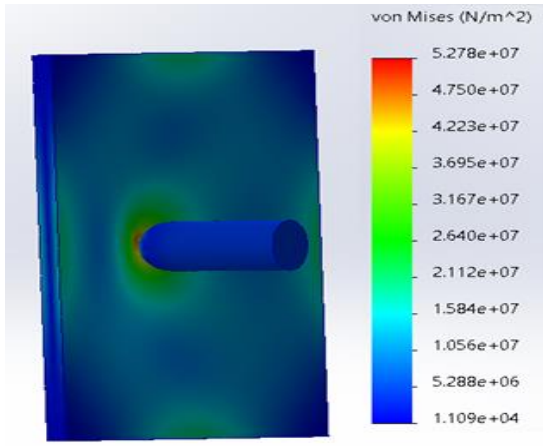

Figure 39. Theoretical simulation results for the composite specimen consist of 15% aluminum powder and 60% glass fiber, shot by a metal mass with a velocity of (16 m/s) to calculate impact stress

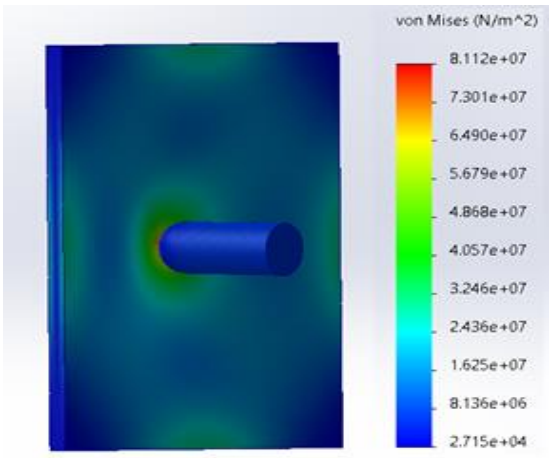

Figure 40. Theoretical simulation results for the composite specimen consist of 15% aluminum powder and 60% glass fiber, shot by metal mass with velocity of (20 m/s) to calculate impact stress

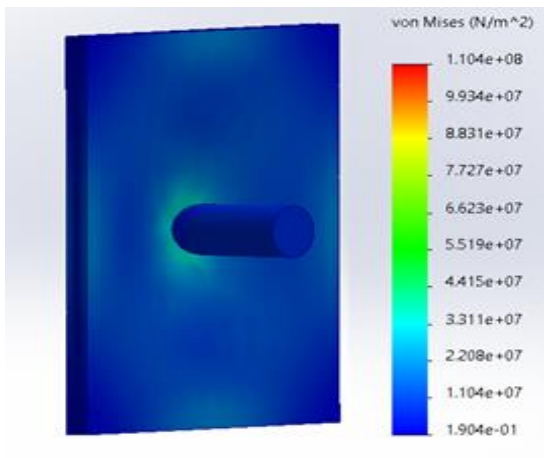

Figure 41. Theoretical simulation results for the composite specimen consist of 15% aluminum powder and 60% glass fiber, shot by metal mass with velocity of (25 m/s) to calculate impact stress

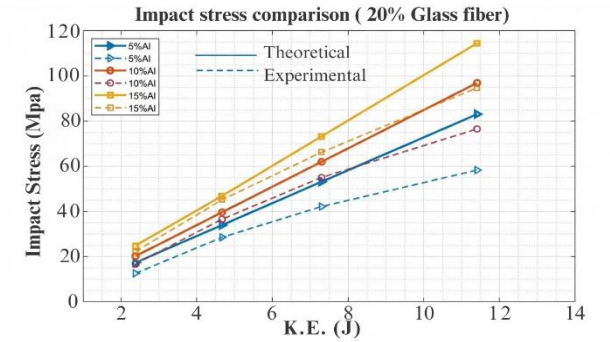

Figure 42. Theoretical and experimental comparison for impact stress effected by composite specimen consist of 5-10-15% and 20% glass fiber

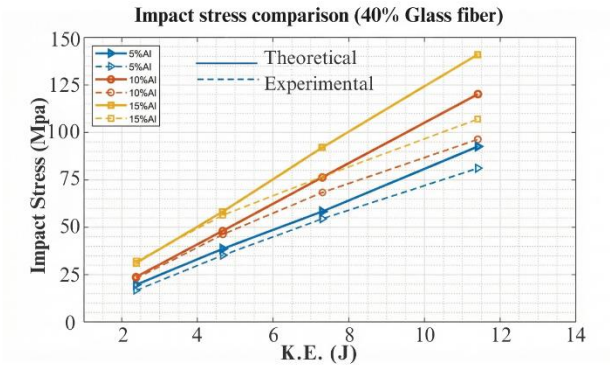

Figure 43. Theoretical and experimental comparison for impact stress affected by composite specimen consist of 5-10-15% and 40% glass fiber

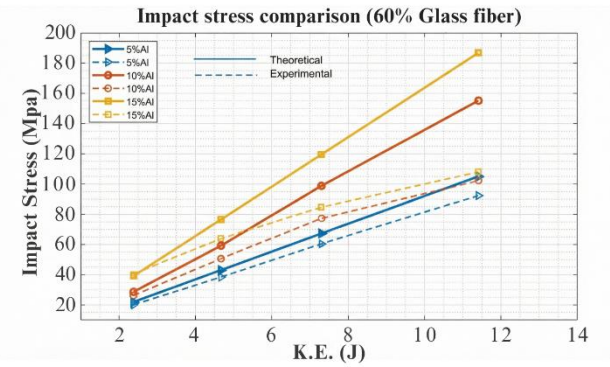

Figure 44. Theoretical and experimental comparison for impact stress effected by composite specimen consist of 5-10-15% and 60% glass fiber

3.5 Comparison of theoretical and experimental results

Figures 42-44 show a comparison between the experimental and theoretical results for impact stress affected by composite specimens consisting of 5-10-15% and 20%, 40%, and 60% glass fiber. The predictions made using standard models for composite materials align well with the experimental findings, especially regarding impact stress and kinetic energy responses. Although the theoretical models effectively depict the behavior of the composite, minor differences between the theoretical outcomes and experimental data can be linked to issues like material imperfections, fiber misalignment, and inconsistencies in the manufacturing process. However, the strong correlation between the theoretical and experimental results confirms the reliability of the models applied in this research.

4. CONCLUSIONS

This study demonstrates that one of the key factors influencing damage resistance is the shape of the nose of the impacting projectile. In this case, the effectiveness of the laminates can be appropriately optimized by adjusting the strength parameters to enhance their design against failure. The conclusion drawn from this study can be summarized as:

1. The findings indicate that a hybrid composite consisting of 10–15% aluminum powder and 60% glass fiber represent the optimal configuration. This combination enhances tensile strength, stiffness, and impact resistance, making it suitable for high-performance applications in fields such as UAV skins and aircraft interior panels, as it offers superior performance across various loading scenarios.
2. The tensile strength and impact resistance of the composite improved with the inclusion of aluminium powder in the specimen formulation. For example, a rise in aluminium content to roughly 15% was more evident. When glass fiber is mixed with aluminum powder, it significantly enhances tensile strength and impact resistance, which in turn boosts the stiffness of the composite.
3. The findings indicated that enhancing the tensile strength and impact resistance with a glass fiber concentration of 60% yielded the optimal performance. This supports the notion that glass fibers significantly enhance the structural integrity of polymer composites, making them appropriate for applications that require durability and resistance to dynamic loads.
4. This work confirmed the precision of the theoretical models by comparing them with empirical data. Particularly in predicting the tensile and impact characteristics of the composites, simulations run with ANSYS matched with experimental data. This shows that FEA is a reliable tool for the design and optimization of composite materials, therefore ensuring that future developments could be faithfully modeled before experimentation.

ACKNOWLEDGMENT

The authors are thankful to the Mechanical Engineering Department and the Prosthetics and Orthotics Engineering Department, College of Engineering, University of Kerbala, Iraq.

REFERENCES

[1] Zan, Y.N., Zhou, Y.T., Li, X.N., Ma, G.N., Liu, Z.Y., Wang, Q.Z., Wang, D., Xiao, B.L., Ma, Z.Y. (2020). Enhancing high-temperature strength and thermal stability of Al2O3/Al composites by high-temperature pre-treatment of ultrafine Al powders. Acta Metallurgica Sinica, 33: 913-921. https://doi.org/10.1007/s40195-020-01038-8

[2] Safri, S.N.A., Sultan, M.T.H., Yidris, N., Mustapha, F. (2014). Low velocity and high velocity impact test on composite materials – A review. The International Journal of Engineering and Science (IJES), 3(9): 50-60.

[3] Mohmmed, J.H., Mahmood, N.Y., Ali, M., Zainulabdeen, A.A. (2020). Buckling and bending properties of aluminium plate with multiple cracks. Archives of Materials Science and Engineering, 106(2): 49-58. https://doi.org/10.5604/01.3001.0014.6972

[4] Asi, O. (2009). Mechanical properties of glass-fiber reinforced epoxy composites filled with Al 2O3 particles. Journal of Reinforced Plastics and Composites, 28(23): 2861-2867. https://doi.org/10.1177/0731684408093975

[5] Ali, M., Mohmmed, J.H., Zainulabdeen, A.A. (2021). Experimental study of the mechanical and corrosion properties of ethyl silicate resin applied on low carbon steel. Archives of Materials Science and Engineering, 108(2): 68-74. https://doi.org/10.5604/01.3001.0015.0255

[6] Megahed, M., Fathy, A., Morsy, D., Shehata, F. (2021). Mechanical performance of glass/epoxy composites enhanced by micro-and nanosized aluminum particles. Journal of Industrial Textiles, 51(1): 68-92. https://doi.org/10.1177/1528083719874479

[7] Ali, M., Alshalal, I., Abtan, A.A., Yousif, A.R., Mohmmed, J.H. (2021). Effect of nano-sized SiO2 particles addition on the surface roughness and micro hardness of copper-based friction materials. Journal of Mechanical Engineering Research and Developments, 44(2): 104-111.

[8] Sarkar, P., Modak, N., Sahoo, P. (2017). Mechanical characteristics of aluminium powder filled glass epoxy composites. International Journal of Engineering and Technologies, 12: 1-14. https://doi.org/10.56431/p-27z4w9

[9] Hasan, I.S., Ali, M., Hussein, E.Q. (2025). Effect of study of composite materials under high-velocity impact. Archives of Materials Science and Engineering, 132(2): 49-58. https://doi.org/10.5604/01.3001.0055.2853

[10] Singh, S., Gupta, P.K. (2022). Effect of fiber orientation on mechanical properties of jute/carbon/glass hybrid composite. Materials Today: Proceedings, 68: 2574-2580. https://doi.org/10.1016/j.matpr.2022.09.419

[11] Ali, M., Hashim, H.A., Oleiwi, A.H., Mohmmed, J.H. (2025). Study of tensile, hardness, and compressive properties of prosthetic pylon made of ramie and carbon/glass hybrid composite materials. Archives of Materials Science and Engineering, 132(1): 21-28. https://doi.org/10.5604/01.3001.0055.2152

[12] Duell, J.M. (2004). Impact testing of advanced composites. Advanced Topics in Characterization of Composites, 97(5): 97-112.

[13] Ali, M., Al-Asadi, N.K.F., Mohmmed, J.H. (2025). Corrosion-induced mechanical properties deterioration in 304L and 316L stainless steels under simulated physiological conditions: A comparative study. Advances in Science and Technology Research Journal, 19(12): 91-99. https://doi.org/10.12913/22998624/210076

[14] Mamoon, A., Al-Jaafari, A. (2020). Fatigue behavior of aluminum sic nano composites material with different reinforcement ratio. IOP Conference Series: Materials Science and Engineering, 870: 012159. https://doi.org/10.1088/1757-899X/870/1/012159

[15] Abdulsahib, R.A., Ali, M., Majeed, M.H. (2025). An experimental investigation of oil jet lubrication effects at various injection angles, cutting parameters, and pressure on surface roughness in different-speed machinery. Archives of Materials Science and Engineering, 133(1): 34-41. https://doi.org/10.5604/01.3001.0055.2916

[16] Stephen, C., Shivamurthy, B., Mourad, A.H.I., Selvam, R., Mohan, M. (2022). Experimental and finite element study on high-velocity impact resistance and energy absorption of hybrid and non-hybrid fabric reinforced polymer composites. Journal of Materials Research and Technology, 18: 5406-5418. https://doi.org/10.1016/j.jmrt.2022.05.007

[17] Rauf, O.U., Khurram, A.A., Hussain, R., Tauqir, A., Hashmi, F., Rehman Shah, O.U., Khokhar, M.S., Shifa, M. (2021). Nanoparticles enhanced interfaces of glass fiber laminate aluminum reinforced epoxy (GLARE) fiber metal laminates. Polymer Composites, 42(8): 3954-3968. https://doi.org/10.1002/pc.26107

[18] Bash, A.M., Othman, T.T., Oleiwi, J.K. (2025). Comparative study on creep, hardness, and density properties of materials for transtibial prosthetic socket fabrication. Tikrit Journal of Engineering Sciences, 32(2): 1-13. https://doi.org/10.25130/tjes.32.2.37

[19] Zainulabdeen, A.A., Mahdi, B.S., Mohmmed, J.H., Abdulkader, N.J., Ali, M. and Flayyih, M.A., 2024. Study of the fatigue fractography of dual phase low carbon steel used in automotive industry. Theoretical and Applied Mechanics Letters, 14(5): 100552. https://doi.org/10.1016/j.taml.2024.100552

[20] Yalcin, E.B., Gunay, V., Marsoglu, M. (2012). Impact behaviour of composite materials by using low and high speed impact tests. Advanced Materials Research, 445: 189-194. https://doi.org/10.4028/www.scientific.net/AMR.445.189